

OXYGEN ABUNDANCES IN LOW SURFACE BRIGHTNESS DISK GALAXIES

STACY S. MCGAUGH^{1,2}

Department of Astronomy, University of Michigan
 Received 1992 August 24; accepted 1993 November 5

ABSTRACT

The oxygen abundances in the H II regions of a sample of low surface brightness (LSB) disk galaxies are presented. In general, LSB galaxies are found to be metal poor ($Z < \frac{1}{3}Z_{\odot}$). Indeed, some LSB galaxies rival the lowest abundance extragalactic objects known, and this sample greatly increases the number of very low metallicity systems known. These low metallicities indicate that LSB galaxies evolve slowly, forming relatively few stars over a Hubble time.

The low metallicities of LSB galaxies occur even though many are comparable in size and mass to the prominent spirals which define the Hubble sequence. As well as being low in surface brightness, these galaxies tend to be isolated. This suggests that surface mass density and environment are more relevant to galaxy evolution than gross size.

Despite the low surface brightness of the disks, massive ($M > 60 M_{\odot}$) stars are inferred to be present and no abnormality of the IMF is indicated. Many low-excitation H II regions exist at low metallicity in LSB galaxies, and the ionization parameter is not tightly correlated with metallicity. However, there does seem to be a significant envelope of maximum ionization at a given metallicity.

Subject headings: galaxies: abundances — galaxies: stellar content — H II regions — ISM: abundances

1. INTRODUCTION

Low surface brightness (LSB) galaxies are an important but often neglected part of the galaxy content of the universe. Their importance stems both from the selection effects which cause them to be underrepresented in galaxy catalogs, and from the clues they contain about the physical processes of galaxy evolution. Here, emphasis is placed on the latter, as probed by the gas phase chemical abundances in LSB galaxies. Although the study of abundances in high surface brightness (HSB) spirals is a well-developed field (e.g., Pagel & Edmunds 1981; McCall, Rybski, & Shields 1985; Torres-Peimbert, Peimbert, & Fierro 1989; Diaz et al. 1991; Vila-Costas & Edmunds 1992), at present only a very little is known about the composition of a limited sample of LSB spirals (Webster et al. 1983).

That LSB galaxies have been neglected is not surprising considering the technical difficulties imposed by their nature. With *peak* surface brightnesses $\mu_0 \geq 23B$ mag arcsec⁻², spectral observations of their stellar continua are virtually impossible because the sky background always dominates the signal. This problem is approached here by concentrating on the emission regions within LSB galaxies for which it is possible, although still difficult, to obtain reasonable quality data.

To this end, spectra of a large sample of H II regions in LSB galaxies have been obtained. The H II regions provide powerful probes of the physical conditions in the galaxies in which they reside. The strong emission lines are more readily observable than the weak continuum, and line ratio diagnostics contain information about the chemical abundances in the gas and the stars which ionize it. These H II regions are almost always giant

H II regions ionized by clusters of stars rather than individual stars.

The H II regions were identified in the disks of LSB galaxies from narrow-band H α images (McGaugh 1992). The sample was selected from the lists of Schombert & Bothun (1988) and Schombert et al. (1992), and from the UGC (Nilson 1973). All of these galaxies have central surface brightnesses well below the canonical Freeman (1970) value of $\mu_0 = 21.65$ mag arcsec⁻², with the sample median being $\mu_0 = 23.4$ mag arcsec⁻² (McGaugh & Bothun 1993). A wide range of morphologies are present, and no single type can be considered representative (see images in McGaugh, Bothun, & Schombert et al. 1994a). Nonetheless, it is not uncommon for the H II regions to be embedded in a weak spiral pattern although there are generally not enough H II regions along the arms to define them as in Sc galaxies.

It is important to realize that while these LSB galaxies are all disk systems of low surface brightness, they are *not* dwarf galaxies. Rather, they are normal size disk galaxies insofar as the scale length distribution of this sample is indistinguishable from that of the HSB spirals which define the Hubble sequence (McGaugh & Bothun 1994). This is an investigation of the properties of typical spiral size disks over a range of surface brightness, not of the relationship between star bursting dwarf galaxies and their presumably LSB progenitors (e.g., Tyson & Scalo 1988).

A de facto selection effect in a study of this kind is the presence of H II regions. While these are more common than might be expected in galaxies selected for low surface brightness, the sample can in no way be considered complete. It nevertheless provides the opportunity to study the physical properties of an interesting if not exhaustive portion of the LSB galaxy population.

2. OBSERVATIONS AND REDUCTIONS

Optical spectra of 71 H II regions in 22 LSB galaxies were obtained over the course of several observing seasons from

¹ Visiting Astronomer, Kitt Peak National Observatory, National Optical Astronomy Observatories, which is operated by Associated Universities for Research in Astronomy, Inc., under cooperative agreement with the National Science Foundation.

² Current address: Institute of Astronomy, University of Cambridge, Madingley Road, Cambridge CB3 0HA, England, UK.
 I: ssm@mail.ast.cam.ac.uk.

1989 September through 1992 February. Blue spectra covering the 3500–5400 Å range were acquired with the Kitt Peak 2.1 m telescope and Gold Camera Spectrograph using a TI 800 × 800 CCD as the detector. Red spectra covering 5700–7000 Å were obtained with the Hiltner 2.4 m telescope, Mk III spectrograph, and TI-4849 CCD (Luppino 1989) of the MDM³ Observatory. Long baseline spectra covering 4500–7300 Å were also obtained at MDM Observatory with this equipment.

Since LSB galaxies and their H II regions generally cannot be seen with the finder cameras of these telescopes, the slit was positioned by offsetting from nearby stars. The offsets were measured from the H α images used to identify the target H II regions. Slit angles were chosen to maximize the number of H II regions which could be observed simultaneously. To minimize the impact of differential atmospheric refraction and the uncertainty in the offset procedure, a wide (3".4) slit was used. This resulted in a resolution of ~ 11 Å for the blue spectra, ~ 8 Å for the red spectra (adequate for splitting [N II] from H α and the [S II] doublet), and ~ 15 Å for the long baseline spectra. These latter overlap the red and blue spectra and were used to place them on the same relative flux scale. The linking spectra also provide a consistency check. Except in a few cases where the offset procedure obviously failed, the line *ratios* agree to within the errors expected from counting statistics and the read noise of the CCD detectors. Because the spectra were not always obtained under photometric conditions, the *fluxes* of individual lines observed multiple times were not always the same. Fortunately, this study requires only line ratios, and is unaffected by uncertainties in the absolute zero point of the flux scale.

Data reduction was accomplished primarily in IRAF.⁴ This began with subtraction of the bias level and dark current. The frames were flattened in the spectral direction with lamp flats, and the slit illumination was made uniform with twilight sky flats. Emission line lamps provided spectral calibration and two-dimensional justification for optimal sky subtraction. Standard star observations were used to flux calibrate the object frames. This latter step also corrected for the spectral shape of the instrumental response. Apertures containing individual H II regions were extracted and stored as one-dimensional spectra. Line fluxes were measured from these by using the FIGARO package to fit Gaussians to the nebular emission lines. The data were subsequently reanalyzed with the improved Gaussian fitting routines in IRAF, recovering the same results within the errors.

The data are presented in Tables 1 and 2. Table 1 contains Balmer emission line data and information derived therefrom. Column (1) contains the galaxy name. Galaxies beginning with "F" are from the lists of Schombert & Bothun (1988) and Schombert et al. (1992) and are designated by sky survey field number. Galaxies beginning with "U" are from the UGC. Column (2) contains the H II region specification (McGaugh 1992). Column (3) contains the observed H β flux in units of 10^{-18} ergs cm⁻² s⁻¹. Because conditions were not always photometric, these numbers may not always be within the formal errors listed in column (4), which include the internal contributions to the uncertainty (the shot noise in the line and continuum and the read noise of the detector), but no estimate

of the uncertainty in the flux calibration. Columns (5), (6), and (7) contain the observed equivalent width in angstroms of the Balmer lines H γ , H β , and H α , respectively. Being a measure of the line relative to the surrounding continuum, these are not subject to uncertainties in the zero point caused by non-photometric conditions. Indeed, the greatest uncertainty here is in the placement of the low continuum level. Column (8) contains the reddening coefficient c , related to the more familiar $E(B-V)$ by $E(B-V) = 0.78c$. The error in c is listed in column (9).

The reddening coefficient is determined from the interstellar extinction curve of Savage & Mathis (1979) with the observed Balmer decrements by assuming case B ratios for a $T_e = 10,000$ K nebula in the low-density limit. This is an adequate assumption, as the ratios of the [S II] lines generally indicate the low-density limit, and the Balmer decrement is not very sensitive to either density or electron temperature. In a few cases of zero reddening and hot nebulae, modestly negative reddenings are derived. These are set to zero in the subsequent analysis.

The derived value of the reddening coefficient is sensitive to the presence of Balmer absorption in the underlying stellar continuum. This alters the Balmer decrement in the same sense as the reddening, so the latter will be overestimated if absorption is present but the departure from the case B ratio is attributed entirely to interstellar reddening. The amount of absorption in any single object is very difficult to estimate, as the solution is always unconstrained. That is, observation of n Balmer lines gives $n - 1$ independent decrements to constrain $n + 1$ variables (the n absorption equivalent widths plus the reddening). This is commonly approached by assuming that the absorption equivalent widths are the same (McCall et al. 1985), or by constructing population synthesis models which are adjusted to subtract away the absorption (see, e.g., Olofsson 1989). While the former approach may be an oversimplification, the latter requires specification of many potentially degenerate parameters (Silva 1991) such as the shape of the star formation history, the age of the star formation event, and the IMF. Such procedures may introduce more systematic uncertainties than they remove.

Although it is difficult to estimate the amount of absorption in individual spectra, the entire sample can be treated in a statistical sense by varying an assumed amount of absorption. In order to avoid the reddenings becoming negative, and introducing a spurious trend of reddening with emission equivalent width, the LSB data require $W_{\lambda}^{\text{abs}} < 4$ Å, and suggest $1 < W_{\lambda}^{\text{abs}} < 3$ Å. Although large amounts of absorption cannot be ruled out in a few individual cases (such as H II region A2 in F746-1 and S1A2 in UGC 6151), it appears to be ~ 2 Å in most LSB H II regions. This is the value found in the H II regions of HSB spirals (McCall et al. 1985; Oey & Kennicutt 1993), so in order to compute the reddening it is assumed that $W_{\lambda}^{\text{abs}} = 2$ Å. Variation from the assumed value is a fundamental systematic uncertainty in this work and all like it. However, the magnitude of the effect is small for the statistically allowed range of absorption, and a more serious (and basic) assumption may be that of the universal applicability of the standard extinction curve.

Table 2 contains the observed fluxes of the important nebular lines. Galaxies and H II regions are specified as per Table 1, followed by the linear intensities of the indicated lines relative to H β (before correction for absorption or reddening) and their uncertainties. The uncertainty in the line ratios includes that in both the relevant line and in H β . In the case of

³ MDM Observatory is operated by the University of Michigan, Dartmouth College, and the Massachusetts Institute of Technology.

⁴ The Image Reduction and Analysis Facility (IRAF) is distributed by the Association of Universities for Research in Astronomy, Inc., under contract to the National Science Foundation.

TABLE 1
BALMER LINE DATA

Galaxy	H II	$F(H\beta)$ $10^{-18} \text{ erg cm}^{-2} \text{ s}^{-1}$	$\sigma_{H\beta}$	$W_\lambda(H\gamma)$ Å	$W_\lambda(H\beta)$ Å	$W_\lambda(H\alpha)$ Å	c	σ_c
F415-3	A1	2964	94	16	35	113	0.383	0.096
F469-2	A1	1368	74	34	50	350	0.168	0.165
F469-2	A2	594	62	12	24	152	0.005	0.311
F469-2	A3	2123	84	21	39	259	0.110	0.121
F469-2	A4	515	60	18	32	152	0.558	0.341
F530-3	A1	1727	79	33	97	466	0.396	0.139
F530-3	A2	509	60	5	26	134	0.075	0.353
F558-1	A1	575	61	...	5	17	0.076	0.288
F558-1	A2	323	56	...	5
F561-1	A1	164	53	...	5	28	-0.007	0.869
F561-1	A2	52	51	13
F561-1	A3	925	67	...	22	49	0.479	0.211
F563-V1	A1	276	56	...	13	49	0.112	0.581
F563-V1	A2	306	56	...	8	44	0.041	0.521
F563-V2	A1	294	56	5	12	32	0.129	0.546
F563-V2	A2	399	58	2	10	48	0.934	0.396
F563-V2	A3	1693	78	9	32	131	0.903	0.134
F568-1	A1	219	54
F568-1	A2	225	55	...	14
F568-6	S1A1	683	63	...	8	97	1.085	0.245
F568-6	S1A2	744	64	...	11	109	0.787	0.238
F568-6	S3A1	62	51	12
F568-6	S3A2	1030	69	5	19	171	0.535	0.192
F568-6	S3A3	140	53	...	14	118	0.908	1.011
F577-V1	A1	213	54	...	25	155	0.588	0.716
F577-V1	A2	128	53	...	7	41	1.377	1.085
F577-V1	A3	1157	71	11	28	164	0.428	0.180
F577-V1	A5	908	67	8	31	130	0.414	0.217
F583-1	A2	166	53	...	10	39	0.220	0.898
F583-1	A3	1502	76	14	47	125	-0.004	0.157
F583-5	A1	753	64	5	13
F583-5	A2	802	65	...	43
F585-3	S1A1	880	66	...	9	152
F585-3	S1A2	1413	74	...	8	48
F585-3	S1A3	368	57	...	8	76
F585-3	S2A1	94	52	...	19
F585-3	S2A2	487	60	...	30
F585-3	S2A3	817	65	...	6
F585-3	S2A4	692	63	...	21
F611-1	A1	1391	74	20	46	303	0.339	0.160
F611-1	A2	788	65	...	53	982	0.159	0.250
F746-1	A1	2864	93	18	53	120	0.294	0.099
F746-1	A2	1524	76	3	12	47	0.674	0.140
F746-1	A3	433	59	...	25
U 1230	A1	392	58	5	45	264	0.195	0.443
U 1230	A2	1045	69	14	28	174	0.167	0.198
U 1230	A3	2218	85	21	51	249	0.165	0.118
U 1230	A4	242	55	8	11	58	0.702	0.625
U 1230	A5	527	60	17	33	101	0.131	0.344
U 5675	A1	263	55	...	9
U 5675	A3	466	59	...	17
U 5709	A1	493	60	...	2	34
U 5709	A2	99	52	57
U 5709	A3	1212	72	...	19	47	0.296	0.173
U 6151	S1A1	3073	96	16	47	148	0.152	0.095
U 6151	S1A2	2742	92	13	33	182	0.667	0.098
U 6151	S3A1	446	59	...	10	...	-0.003	0.197
U 6151	S3A2	1839	80	...	56	424	-0.004	0.055
U 6614	A1	298	56	...	7
U 6614	A2	258	55	...	9
U 6614	A3	244	55	...	9
U 9024	S1A1	1238	72	23	61	...	0.477	1.013
U 9024	S1A2	857	66	...	29
U 9024	S1A3	266	55	...	20
U 9024	S2A1	1369	74	...	54
U12695	S1A1	999	68	27	93	346	0.133	0.210
U12695	S1A2	3411	99	11	44	265	0.158	0.089
U12695	S1A3	1118	70	25	74	338	-0.095	0.197
U12695	S2A1	3611	102	38	91	...	0.047	0.411
U12695	S2A2	3730	103	19	61	173	0.140	0.085
U12695	S2A3	1667	78	16	51	...	0.138	0.431

TABLE 2
 LINE RATIOS

Galaxy	H II	[O II]		[Ne III]		H γ		[O III]		[O III]	
		$\lambda 3727$	σ_λ	$\lambda 3869$	σ_λ	$\lambda 4341$	σ_λ	$\lambda 4363$	σ_λ	$\lambda 4959$	σ_λ
F415-3	A1	2.37	0.09	0.45	0.03	0.50	0.13	<0.11	...	1.03	0.05
F469-2	A1	2.06	0.13	0.26	0.14	0.68	0.16	0.09	0.04	0.81	0.07
F469-2	A2	1.63	0.20	0.42	0.20	0.60	0.21	0.88	0.13
F469-2	A3	1.30	0.07	0.38	0.03	0.59	0.14	0.14	0.02	1.79	0.08
F469-2	A4	1.68	0.23	0.73	0.14
F530-3	A1	1.20	0.07	0.38	0.04	0.40	0.04	0.14	0.03	1.39	0.08
F530-3	A2	0.23	0.10	0.10	0.10	1.68	0.23
F558-1	A1	4.97	0.55	0.76	0.13	0.58	0.11
F558-1	A2	5.32	0.97
F561-1	A1	2.71	0.96	0.66	0.38
F561-1	A2	2.81	2.94
F561-1	A3	3.13	0.25	0.51	0.07	0.06	0.05	0.79	0.09
F563-V1	A1	2.71	0.59	1.84	0.43
F563-V1	A2	0.86	0.24	0.57	0.20
F563-V2	A1	1.46	0.34	0.36	0.19	0.49	0.20	0.49	0.20
F563-V2	A2	3.08	0.48	0.27	0.13	0.92	0.19
F563-V2	A3	2.51	0.13	0.38	0.04	0.39	0.04	0.03	0.03	1.05	0.06
F568-1	A1	1.48	0.45	0.56	0.28
F568-1	A2	3.03	0.79	0.80	0.31
F568-6	S1A1	3.22	0.32	0.32	0.08
F568-6	S1A2	2.01	0.20	0.27	0.07
F568-6	S3A1	8.42	7.12
F568-6	S3A2	2.81	0.21	0.19	0.08	0.30	0.05	0.27	0.05
F568-6	S3A3	4.74	1.86	0.39	0.39
F577-V1	A1	3.78	0.99	0.72	0.30
F577-V1	A2	4.69	2.01	1.72	0.83
F577-V1	A3	4.32	0.28	0.21	0.08	0.47	0.06	0.01	0.04	1.00	0.08
F577-V1	A5	3.96	0.31	0.31	0.11	0.34	0.06	<0.10	...	1.45	0.13
F583-1	A2	4.15	1.40	0.89	0.43
F583-1	A3	1.35	0.08	<0.52	...	0.30	0.04	0.02	0.03	1.72	0.10
F583-5	A1	2.73	0.26	0.46	0.18	1.09	0.12
F583-5	A2	0.70	0.09	1.10	0.12
F585-3	S1A1	3.48	0.28	<0.36	1.34	0.13
F585-3	S1A2	3.03	0.17	0.48	0.25	1.38	0.09
F585-3	S1A3	3.87	0.64	0.84	0.20
F585-3	S2A1	4.27	2.47	0.75	0.69
F585-3	S2A2	2.75	0.37	1.07	0.18
F585-3	S2A3	3.82	0.32	<0.71	1.19	0.12
F585-3	S2A4	2.28	0.23	1.18	0.14
F611-1	A1	1.54	0.10	0.46	0.05	<0.14	...	1.14	0.08
F611-1	A2	1.25	0.13	0.42	0.18	0.76	0.10
F746-1	A1	3.36	0.12	0.79	0.03	0.38	0.02	1.30	0.05
F746-1	A2	5.97	0.31	1.44	0.09	0.31	0.04	0.08	0.05	1.08	0.07
F746-1	A3	3.87	0.55	1.11	0.20	1.15	0.21
U 1230	A1	2.13	0.36	0.15	0.13	0.87	0.19
U 1230	A2	2.64	0.19	0.57	0.27	0.12	0.05	0.86	0.08
U 1230	A3	2.01	0.09	0.13	0.07	0.46	0.06	<0.26	...	0.94	0.05
U 1230	A4	2.97	0.73	0.78	0.38	1.60	0.43
U 1230	A5	0.83	0.74	0.39	0.14	0.50	0.22	1.69	0.23
U 5675	A1	5.70	1.24	0.59	0.24
U 5675	A3	3.48	0.44	0.69	0.14
U 5709	A1	4.03	2.51	0.52	0.13
U 5709	A2	6.30	3.03	1.24	0.75
U 5709	A3	2.35	0.15	0.60	0.06
U 6151	S1A1	3.76	0.12	0.33	0.12	0.42	0.02	0.97	0.04
U 6151	S1A2	4.16	0.15	0.42	0.02	0.46	0.03	0.13	0.02	1.05	0.04
U 6151	S3A1	11.44	1.54	0.35	0.12
U 6151	S3A2	3.16	0.16	0.22	0.03
U 6614	A1	1.62	0.36	0.10	0.17
U 6614	A2	1.82	0.45	0.20	0.20
U 6614	A3	1.17	0.35	0.06	0.20
U 9024	S1A1	2.43	0.16	0.68	0.26	0.38	0.05	<0.12	...	1.59	0.11
U 9024	S1A2	3.27	0.27	0.59	0.08
U 9024	S1A3	2.69	0.61	0.45	0.22
U 9024	S2A1	3.00	0.18	1.06	0.07
U12695	S1A1	1.14	0.10	0.55	0.17	0.45	0.06	0.01	0.05	1.31	0.11
U12695	S1A2	2.01	0.07	0.43	0.12	0.35	0.02	0.03	0.02	1.37	0.05
U12695	S1A3	1.77	0.13	0.46	0.16	0.41	0.05	1.58	0.12
U12695	S2A1	0.73	0.03	0.44	0.12	0.44	0.02	0.12	0.02	1.78	0.06
U12695	S2A2	1.90	0.06	0.31	0.12	0.43	0.02	0.06	0.01	1.15	0.04
U12695	S2A3	1.90	0.10	0.26	0.13	0.43	0.04	0.06	0.03	1.52	0.08

object A2 in UGC 5709 and S3A1⁵ in F568-6, H β is only marginally detected so the listed error is large, but the ratios of

⁵ This is the only object in the sample which is not obviously an H II region. It is not prominent in *U* (see image in McGaugh et al. 1994a), suggesting that local photoionization is not responsible for the observed emission. The spectrum is consistent with very low excitation photoionization or shock heating, so it may be that this object is a jet originating in or photoionized by the AGN in this giant galaxy (Bothun et al. 1990).

the other lines to one another are rather more certain. For important marginal detections and significant nondetections, an upper limit denoted by a less than sign is given. It should also be noted that the measurements of [O III] $\lambda 4959$ and [O III] $\lambda 5007$ are not strictly independent, as they were initially constrained to be in their theoretical ratio. This constraint on the fit was subsequently relaxed, but the fit to these lines usually did not change much.

TABLE 2—Continued

Galaxy	H II	[O III]		H α		[N II]		[S II]		[S II]	
		$\lambda 5007$	σ_λ	$\lambda 6563$	σ_λ	$\lambda 6583$	σ_λ	$\lambda 6717$	σ_λ	$\lambda 6731$	σ_λ
F415-3	A1	3.62	0.13	4.03	0.14	0.15	0.02	0.27	0.02	0.21	0.02
F469-2	A1	2.36	0.14	3.37	0.20	0.14	0.04	0.21	0.04	0.17	0.04
F469-2	A2	2.70	0.31	2.97	0.33	<0.13	...	0.18	0.09	0.28	0.09
F469-2	A3	5.81	0.24	3.22	0.14	0.07	0.02	0.15	0.02	0.14	0.02
F469-2	A4	1.24	0.19	4.72	0.58	0.28	0.10
F530-3	A1	3.88	0.19	4.06	0.20	0.19	0.03	0.44	0.04	0.27	0.03
F530-3	A2	3.65	0.46	3.14	0.40	0.15	0.10	0.20	0.10	0.044	0.10
F558-1	A1	1.29	0.17	3.27	0.37	0.59	0.11
F558-1	A2	0.30	0.17
F561-1	A1	2.44	0.87	2.94	1.03	<0.22	...	0.43	0.34	0.60	0.37
F561-1	A2	5.38	5.39	3.73	3.81
F561-1	A3	2.37	0.19	4.35	0.33	<0.19	...	0.66	0.08	0.53	0.07
F563-V1	A1	4.42	0.93	3.27	0.70	<0.08
F563-V1	A2	1.70	0.37	3.27	0.64	<0.09	...	0.31	0.18	0.23	0.17
F563-V2	A1	1.20	0.30	3.28	0.67	<0.23	...	0.96	0.26	0.63	0.22
F563-V2	A2	3.04	0.48	6.73	1.01	<0.67	...	1.21	0.23	1.02	0.21
F563-V2	A3	3.03	0.15	6.32	0.31	0.28	0.03	0.88	0.06	0.73	0.05
F568-1	A1	1.69	0.50
F568-1	A2	2.40	0.64
F568-6	S1A1	0.96	0.12	8.01	0.76
F568-6	S1A2	0.83	0.11	6.01	0.54
F568-6	S3A1	4.30	3.72	2.13	1.98	1.39	1.44	0.40	0.89
F568-6	S3A2	0.81	0.08	4.73	0.33	1.28	0.11	0.82	0.08	0.15	0.05
F568-6	S3A3	1.17	0.58	6.86	2.66	2.11	0.90	0.90	0.51	1.09	0.56
F577-V1	A1	2.06	0.58	4.88	1.26
F577-V1	A2	5.13	2.19	10.05	4.21	<0.66	...	2.55	1.15	3.30	1.44
F577-V1	A3	2.99	0.20	4.24	0.27	0.34	0.05	0.68	0.07	0.46	0.06
F577-V1	A5	4.21	0.33	4.17	0.32	<0.37
F583-1	A2	2.67	0.93	3.64	1.23
F583-1	A3	5.14	0.27	2.87	0.16
F583-5	A1	3.26	0.30
F583-5	A2	3.28	0.29
F585-3	S1A1	3.99	0.32	3.01	0.25	<0.07
F585-3	S1A2	4.13	0.23	3.01	0.17	0.35	0.04	0.43	0.04	0.34	0.04
F585-3	S1A3	3.26	0.54	3.01	0.50	0.41	0.15	0.39	0.15	0.56	0.17
F585-3	S2A1	2.51	1.52
F585-3	S2A2	3.43	0.45
F585-3	S2A3	4.15	0.35
F585-3	S2A4	3.43	0.34
F611-1	A1	3.45	0.20	3.91	0.22	0.24	0.04	0.36	0.04	0.17	0.04
F611-1	A2	2.68	0.24	3.36	0.30	0.11	0.06	0.17	0.06	0.12	0.06
F746-1	A1	4.06	0.14	3.71	0.13	<0.11
F746-1	A2	3.23	0.17	5.30	0.28	0.61	0.05	0.96	0.06	0.87	0.06
F746-1	A3	3.03	0.44
U 1230	A1	2.06	0.35	3.45	0.54	<0.13	...	0.45	0.15	0.30	0.14
U 1230	A2	2.75	0.20	3.40	0.24	0.28	0.05	0.42	0.06	0.27	0.05
U 1230	A3	2.51	0.11	3.35	0.14	0.26	0.02	0.33	0.03	0.28	0.03
U 1230	A4	3.92	0.94	5.52	1.30	<0.17	...	0.37	0.23	0.48	0.24
U 1230	A5	4.88	0.58	3.25	0.40	0.22	0.10	0.31	0.10	0.28	0.10
U 5675	A1	1.78	0.44
U 5675	A3	2.70	0.35
U 5709	A1	1.57	0.23	2.89	0.38	0.73	0.14
U 5709	A2	3.70	1.83	9.83	4.69	3.11	1.55
U 5709	A3	1.80	0.12	3.75	0.24	0.93	0.08
U 6151	S1A1	2.96	0.10	3.31	0.11	<0.28	...	0.56	0.03	0.36	0.02
U 6151	S1A2	3.09	0.11	5.18	0.18	0.18	0.02	0.94	0.04	0.55	0.03
U 6151	S3A1	1.05	0.19	2.86	0.41	<0.11	...	0.50	0.14	0.34	0.12
U 6151	S3A2	0.64	0.05	3.10	0.16	<0.16	...	0.43	0.04	0.21	0.03
U 6614	A1	0.31	0.18
U 6614	A2	0.61	0.24
U 6614	A3	0.19	0.21
U 9024	S1A1	4.75	0.29
U 9024	S1A2	2.25	0.19
U 9024	S1A3	1.34	0.35
U 9024	S2A1	3.16	0.18
U12695	S1A1	3.98	0.29	3.24	0.24	<0.07	...	0.12	0.05	0.09	0.05
U12695	S1A2	3.91	0.12	3.35	0.10	0.07	0.01	0.19	0.05	0.13	0.05
U12695	S1A3	4.33	0.29	2.65	0.18	0.04	0.03	0.08	0.04	0.06	0.04
U12695	S2A1	5.39	0.16
U12695	S2A2	3.27	0.10	3.26	0.10	<0.09	...	0.36	0.05	0.26	0.11
U12695	S2A3	4.40	0.22

3. ANALYSIS

Figure 1 shows an example H II region spectrum with the important nebular lines identified. Note that this is not a typical spectrum; it is one of the better obtained and is chosen to illustrate the relevant lines. Many H II regions in this sample are too faint for any but the strongest lines to be measured with confidence. In particular, while the [O III] $\lambda 4363$ line is some-

times visible, it is generally not observed with sufficiently high signal to noise for a reliable electron temperature to be determined. This makes the uncertainties in the abundances derived from the nebular spectra using standard methods (Osterbrock 1989) intolerably high.

To overcome this difficulty, the empirical abundance indicating line ratio $R_{23} \equiv ([\text{O II}] \lambda 3727 + [\text{O III}] \lambda \lambda 4959, 5007) / \text{H}\beta$ first discussed by Pagel et al. (1979), as calibrated by

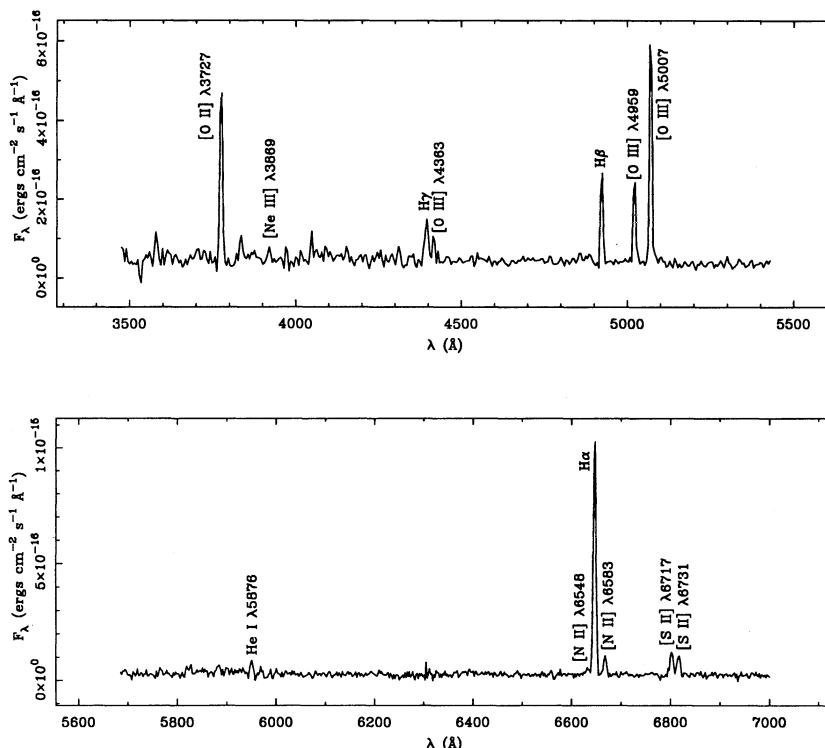


FIG. 1.—Spectrum of H II region A3 in UGC 1230 with important nebular emission lines labeled. This spectrum is chosen for illustration because all the relevant lines are visible. Usually the weak lines [O III] $\lambda 4363$, He I $\lambda 5876$, and [N II] $\lambda 6548$ are not detected, and [N II] $\lambda 6583$ is generally weaker than it is here. Although [O III] $\lambda 4363$ is detected, it is unphysically large. This can be caused by the shocks likely to be present within H II regions (Peimbert, Sarmiento, & Fierro 1991), but in this case is probably just a result of low signal to noise. Empirical methods of estimating the oxygen abundance utilizing the bright R_{23} lines are superior to directly measuring the electron temperature with $\lambda 4363$ until quite high signal to noise is obtained in this faint line.

McGaugh (1991), is employed. An important aspect of this calibration is the recognition of the influence of the ionization parameter at low abundances. When this is considered, the R_{23} method rivals the precision of the standard method when an accurate, direct measure of the electron temperature is available, but has the advantage of relying only on the strongest nebular lines.

3.1. Oxygen Abundances from the Strong Line Method

Figure 2 shows the reddening corrected data for LSB H II regions plotted on the model grid of McGaugh (1991). The oxygen abundance and volume averaged nebular ionization parameter $\langle U \rangle$ (essentially the ratio of ionizing photon density to particle density) can be extracted from this plot. While R_{23} alone is sufficient for determining the oxygen abundance on the upper branch (i.e., the solid lines of constant abundance in Figure 2 are nearly vertical), this is not the case on the lower branch. Here R_{23} depends on $\langle U \rangle$ as well as on abundance, so these must be determined simultaneously. This is accomplished by plotting the ionization sensitive line ratio $O_{32} \equiv ([\text{O III}] \lambda\lambda 4959, 5007)/([\text{O II}] \lambda 3727)$ as the ordinate of Figure 2. While both O_{32} and R_{23} depend on both $\langle U \rangle$ and oxygen abundance on the lower branch, together they contain sufficient information to determine both, and have the further advantage of involving the same strong lines observable in the same wavelength region.

The nebular parameters (O/H, $\langle U \rangle$) are extracted from Figure 2 by the projection of the positions of the data in the observed (R_{23} , O_{32}) plane into the (O/H, $\langle U \rangle$) plane represented by the grid lines. The error in the derived parameters due to

observational uncertainty is taken from the corresponding projection of the error ellipse. The error bars in Figure 2 are computed by propagating the uncertainty in the individual line measurements and the reddening through to the plotted quantity. Objects with excessively large errors are excluded from both the plot and further analysis. The uncertainty in the final values of (O/H, $\langle U \rangle$) are taken from the combination (in quadrature) of the observational uncertainty determined in this fashion and the theoretical uncertainty in the actual position of the grid.

This uncertainty in the calibration varies with abundance. On the upper branch (the solid-lined surface of Fig. 2), R_{23} is accurate to ~ 0.1 dex in $\log(\text{O}/\text{H})$ (which is the separation between the grid lines). The uncertainty in $\langle U \rangle$ on the upper branch is ~ 0.15 dex. The uncertainty in both grows larger above solar abundance as many complicating effects come into play: opacity becomes significant in important cooling lines, the models become sensitive to assumed abundance ratios, and variations in density and ionization cease to be homologous (see Oey & Kennicutt 1993). Also, $\langle U \rangle$ is likely to be systematically affected at large abundances by the lack of metal edges in the model stellar atmospheres, which affects the computed [O III]/[O II] ratio. Fortunately, virtually all LSB galaxies are on the lower branch (the dashed surface of Fig. 2), as will be shown. Here these uncertainties are unimportant. The lower branch calibration is accurate to ~ 0.05 dex in oxygen abundance and ~ 0.1 dex in ionization parameter. For those objects in which [O III] $\lambda 4363$ is observed, the two methods are in agreement within the errors, though the R_{23} method tends to give slightly higher abundances. A complete discussion of the

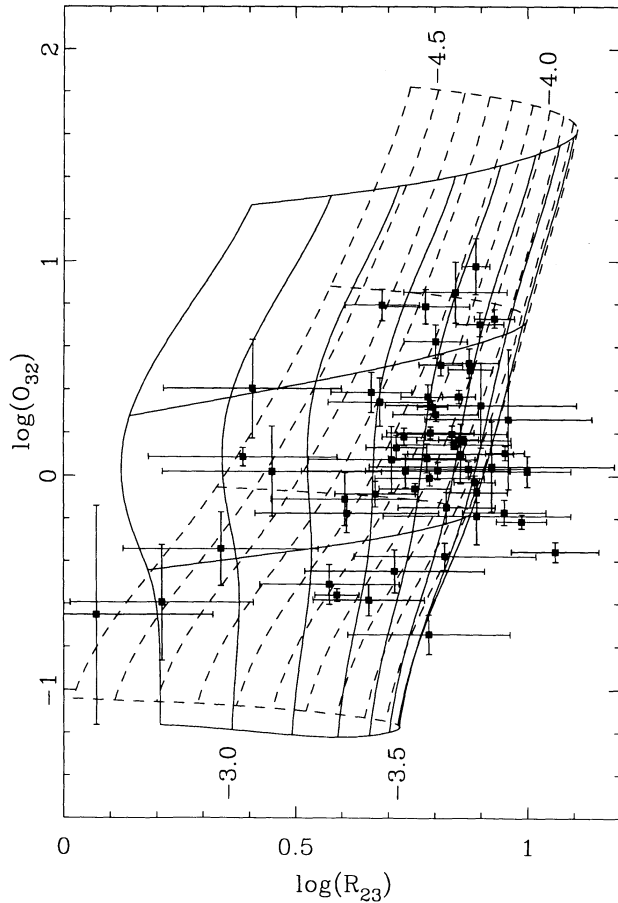


FIG. 2.—LSB H II region data (solid squares) plotted against the model grid of McGaugh (1991). Solid lines refer to the upper branch [$\log(\text{O}/\text{H}) \geq -3.6$] of the R_{23} calibration, while dashed lines define the lower branch. Vertical lines of constant abundance are separated by 0.1 in $\log(\text{O}/\text{H})$. Several of these lines are labeled by the corresponding value of $\log(\text{O}/\text{H})$. Horizontal lines of constant ionization parameter are separated by 1 in $\log\langle U \rangle$ and range from $\log\langle U \rangle = -4$ at the bottom to $\log\langle U \rangle = -1$ at the top. This grid is for a set of H II regions ionized by a cluster IMF with $M_u = 60 M_\odot$. A larger M_u would shift the grid to the right slightly, while a smaller M_u would shift it to the left.

uncertainties in the calibration and a comparison to abundances determined with a direct measurement of the electron temperature is given by McGaugh (1991).

A systematic uncertainty which is not included in the estimate of the error in O/H and $\langle U \rangle$ is the amount of underlying Balmer absorption. As discussed above, this is assumed to be $W_\lambda^{\text{abs}} = 2 \text{ \AA}$. The assumed value affects the flux of H β , and through it, the derived value of the reddening. Increasing the amount of absorption increases the inferred strength of H β relative to the forbidden lines, pushing the data to the left in Figure 2. There is also a small upward component to this vector as $[\text{O III}]/[\text{O II}]$ will increase as the reddening estimate drops. This motion is of course largest for those objects with the smallest observed emission equivalent widths. Varying the assumed value of the absorption over the allowed (0–4 \AA) range does not move most of the data outside the error estimates determined above.

Physically, the empirical method works as an abundance indicator because of the response of the R_{23} lines to electron temperature (Pagel et al. 1979). As the abundance of coolant drops, the nebula becomes hotter and the optical oxygen lines

increase in strength as they bear a growing fraction of the cooling burden. This cannot continue indefinitely, as there must be a point where the oxygen line strengths begin to decrease because oxygen becomes scarce (Edmunds & Pagel 1984). The maximum in R_{23} occurs around $\log(\text{O}/\text{H}) \approx -3.6$ ($\sim 30\%$ of solar), where the lines of constant oxygen abundance in Figure 2 become closely bunched. This bunching severely limits the accuracy of the R_{23} method for objects near the fold, so the abundance can only be determined to be within ~ 0.2 dex of $\log(\text{O}/\text{H}) = -3.6$. Many H II regions inhabit this region of the R_{23} – O_{32} diagram, which causes a somewhat artificial crowding of values near $\log(\text{O}/\text{H}) = -3.6$. This point should be kept in mind when interpreting abundances determined in this fashion.

An important result follows directly from casual inspection of Figure 2. A number of points fall to the right of the fold, outside the range occupied by the model grid. This grid is for H II regions ionized by stellar clusters with an IMF truncated at $M_u = 60 M_\odot$. A grid for $M_u = 100 M_\odot$ would be displaced slightly to the right, bringing the ridge line of the fold into agreement (within the errors) with almost all the data. This is a strong indication that hot ($T_* > 50,000 \text{ K}$), high-mass stars are present in many low surface brightness galaxies. This is consistent with the often large ionizing luminosities implied by the H β fluxes in Table 1. If M_u had a relatively low value ($\sim 30 M_\odot$), satisfying the ionizing luminosity requirement would require so many stars that the restriction on optical surface brightness would be violated. Although the precise value of M_u is model dependent, the spectra indicate stellar temperatures comparable to those in starbursting compact galaxies (Campbell 1988) which have been cited as evidence for a metallicity-dependent IMF (Terlevich 1985). This would imply an IMF biased toward high-mass stars in LSB galaxies, although other lines of evidence suggest, if anything, an IMF lacking in massive stars (Romanishin, Strom, & Strom 1983; Schombert et al. 1990). Consideration of the effects of metallicity on stellar temperature shows that a fixed IMF adequately explains the observed trends in the spectra (McGaugh 1991), so no variation in the IMF is inferred.

That there is a fold in the grid results in an ambiguity. While R_{23} and O_{32} specify O/H and $\langle U \rangle$ with good precision on both branches, they do not specify which branch is appropriate. That is, the surface represented by solid and dashed lines in Figure 2 overlap, so that the values of (O/H, $\langle U \rangle$) corresponding to any observed (R_{23} , O_{32}) are twofold degenerate. This means that two very different H II regions might have identical (R_{23} , O_{32}).

Fortunately, the easily observable line $[\text{N II}] \lambda 6583$ can resolve the degeneracy. It is strong at high abundance, and quite weak at low abundance. Skillman (1989) suggested using it in the form of the empirical abundance indicator $[\text{O III}]/[\text{N II}]$ of Alloin et al. (1979). This line ratio varies monotonically with abundance, but is also sensitive to $\langle U \rangle$. A superior ratio for this purpose is $[\text{N II}]/[\text{O II}]$. This also varies monotonically with oxygen abundance, but is much less sensitive to $\langle U \rangle$, and is observed to form a very narrow sequence over a large range of metallicity (McCall et al. 1985; see Fig. 3). Indeed, $[\text{N II}]/[\text{O II}]$ would be superior to R_{23} as an abundance indicator if the N/O ratio were known a priori. This is not the case, as N/O varies in a complicated fashion with O/H (e.g., Matteucci 1986; Vila-Costas & Edmunds 1993). Nevertheless, it is adequate to clearly distinguish between the upper and lower branches. In Figure 3, the division between upper and

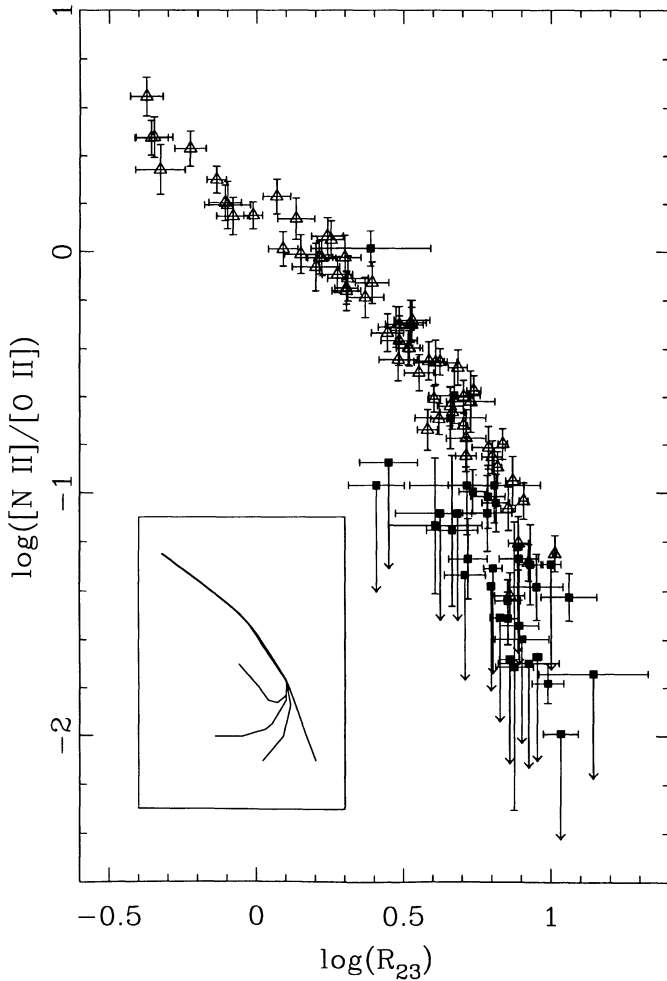


FIG. 3.— $[\text{N II}] \lambda 6583/[\text{O II}] \lambda 3727$ plotted against the abundance indicating line ratio R_{23} . The open triangles are data for HSB spirals from McCall et al. (1985). Solid squares are data for LSB galaxies. The LSB data begin where the HSB data trail off. The transition through the R_{23} turnover region occurs around $\log([\text{N II}]/[\text{O II}]) \approx -1$, so the majority of LSB galaxies are on the lower branch. *Inset:* The theoretically expected behavior of these line ratios. Above $\log([\text{N II}]/[\text{O II}]) \approx -1$, a narrow sequence is anticipated as neither abscissa nor ordinate is very sensitive to either the ionization parameter or the shape of the ionizing spectrum: this is a single parameter sequence in metallicity. Below this value, the scatter in the data is expected to increase due to the sensitivity of R_{23} to $\langle U \rangle$ on the lower branch. The exact path of models with constant $\langle U \rangle$ depends on the N/O abundance ratio, which varies in a complicated way with O/H. Various possibilities are illustrated.

lower branches (the fold in Figure 2) occurs around $\log([\text{N II}]/[\text{O II}]) \approx -1$. H II regions in HSB spirals mostly have $[\text{N II}]/[\text{O II}]$ equal to or larger than this value (i.e., are on the upper branch; see the data of McCall et al. 1985). In contrast, the majority of LSB H II regions have $[\text{N II}]/[\text{O II}]$ weaker than this, indicating that they are on the lower, dashed surface of Figure 2. That the narrow sequence defined by the HSB data disperses as $\log([\text{N II}]/[\text{O II}])$ decreases past -1 is expected from the fact that the abscissa R_{23} is sensitive to $\langle U \rangle$ on the lower branch, and also results from variation in the N/O ratio.

It is an interesting coincidence that the transition between HSB and LSB samples occurs approximately at the turnover in the R_{23} relation. However, this cannot be physically significant. The turnover is defined by local nebular physics, independent of any knowledge of the type of galaxy in which the H II

region is embedded. Indeed, that the samples just overlap suggests that there is a continuum of development histories in disk galaxies, and that surface brightness selection effects place limits on the range of our awareness of these.

3.2. Results

The results of the analysis are presented in Table 3. Galaxies and H II regions are specified as before. Entries are logarithmic, with abundances by number relative to hydrogen. The uncertainties are determined as described above, with observational and calibration uncertainties combined in quadrature. For a few objects in the turnover region with large errors, an abundance is adopted which is the midpoint of the extent of the error bars on either branch. These tend to be slightly less than the approximately -3.6 fold in Figure 2 as the lines of constant abundance are more closely bunched on the lower branch surface.

Because of bad weather, not all galaxies that were observed in the blue (where the R_{23} lines are) were also observed in the red (where the $[\text{N II}]$ line is), and in a few cases the observed limit on $[\text{N II}]$ is not sufficiently restrictive to resolve the branch ambiguity. If no other indicator (such as the presence of $[\text{O III}] \lambda 4363$) of the appropriate branch is available, then the abundances determined from (R_{23}, O_{32}) remain ambiguous. Table 4 contains the possible oxygen abundances for those galaxies for which this is the case. Only one Balmer line is observed in most of these objects, so the reddening is assumed to be equal to the galactic value. A large (0.5 in c) random error is subsumed in the error estimate, but there is obviously no guarantee that the actual abundance determination is not more seriously affected.

TABLE 3
LSB ABUNDANCES

Galaxy	H II	O/H	σ_O	$\langle U \rangle$	σ_U
F415-3	A1	-3.94	0.11	-2.65	0.11
F469-2	A1	-4.17	0.11	-2.73	0.12
F469-2	A2	-4.29	0.21	-2.53	0.17
F469-2	A3	-3.98	0.11	-2.07	0.11
F469-2	A4	-4.24	0.25	-3.02	0.15
F530-3	A1	-4.14	0.09	-2.29	0.11
F561-1	A3	-3.86	0.23	-3.03	0.13
F563-V1	A1	-3.90	0.37	-2.46	0.21
F563-V1	A2	-4.67	0.25	-2.49	0.22
F563-V2	A1	-4.48	0.30	-2.91	0.23
F563-V2	A2	-3.60	0.49	-3.01	0.24
F563-V2	A3	-3.60	0.30	-2.91	0.20
F568-6	S1A1	-3.60	0.36	-3.57	0.25
F568-6	S3A2	-3.22	0.28	-3.30	0.27
F577-V1	A3	-3.60	0.20	-3.00	0.21
F577-V1	A5	-3.60	0.20	-2.81	0.22
F583-1	A3	-4.04	0.13	-2.09	0.11
F585-3	S1A1	-3.92	0.20	-2.67	0.11
F611-1	A1	-4.14	0.12	-2.46	0.11
F611-1	A2	-4.33	0.13	-2.50	0.15
F746-1	A1	-3.60	0.20	-2.86	0.20
F746-1	A2	-3.60	0.30	-3.14	0.30
F746-1	A3	-3.82	0.28	-2.81	0.11
U 1230	A1	-4.17	0.30	-2.80	0.20
U 1230	A2	-4.04	0.16	-2.77	0.13
U 1230	A3	-4.16	0.09	-2.66	0.11
U 1230	A4	-3.66	0.47	-2.78	0.28
U 5675	A1	-3.64	0.46	-3.13	0.23
U 5709	A1	-3.02	0.70	-2.40	0.70
U 5709	A3	-3.21	0.13	-2.70	0.40
U 6151	S1A1	-3.65	0.31	-2.85	0.20
U 6151	S1A2	-3.60	0.25	-3.04	0.25
U 6151	S3A1	-3.60	0.20	-3.70	0.20
U 6151	S3A2	-4.08	0.09	-3.46	0.11
U 9024	S1A1	-3.70	0.36	-2.46	0.20
U12695	S1A1	-4.20	0.12	-2.20	0.15
U12695	S1A2	-4.02	0.09	-2.46	0.12
U12695	S1A3	-4.02	0.15	-2.30	0.13
U12695	S2A1	-4.14	0.08	-1.82	0.17
U12695	S2A2	-4.11	0.08	-2.50	0.11
U12695	S2A3	-4.01	0.12	-2.31	0.10

TABLE 4
 AMBIGUOUS ABUNDANCE DETERMINATIONS

Galaxy	H II	Lower Branch				Upper Branch			
		O/H	σ_O	$\langle U \rangle$	σ_U	O/H	σ_O	$\langle U \rangle$	σ_U
F558-1	A1	-3.92	0.30	-3.35	0.14	-3.28	0.22	-3.17	0.22
F568-1	A2	-4.10	0.31	-2.85	0.22	-3.27	0.22	-2.62	0.21
F583-5	A1	-4.08	0.20	-2.65	0.10	-3.31	0.16	-2.44	0.16
F583-5	A2	-4.41	0.18	-2.09	0.17	-3.16	0.18	-1.64	0.21
F585-3	S1A2	-4.28	0.26	-2.06	0.12	-3.24	0.14	-1.72	0.17
F585-3	S1A3	-3.98	0.26	-2.85	0.11	-3.35	0.19	-2.70	0.16
F585-3	S2A2	-4.00	0.21	-2.64	0.11	-3.36	0.18	-2.45	0.16
F585-3	S2A3	-3.95	0.24	-2.70	0.10	-3.38	0.21	-2.52	0.15
F585-3	S2A4	-4.10	0.23	-2.53	0.17	-3.32	0.21	-2.31	0.24
U 1230	A5	-4.19	0.30	-1.98	0.30	-3.30	0.30	-1.69	0.30
U 5675	A3	-3.99	0.20	-2.85	0.12	-3.33	0.16	-2.68	0.17
U 6614	A1	-4.51	0.23	-3.59	0.27	-2.91	0.19	-3.31	0.40
U 6614	A2	-4.48	0.27	-3.30	0.22	-2.99	0.20	-2.94	0.29
U 6614	A3	-4.65	0.27	-3.63	0.38	-2.84	0.20	-3.25	0.75
U 9024	S1A2	-4.03	0.21	-2.94	0.17	-3.29	0.22	-2.74	0.20
U 9024	S1A3	-4.21	0.32	-3.10	0.13	-3.16	0.23	-2.83	0.19
U 9024	S2A1	-3.95	0.21	-2.69	0.17	-3.39	0.18	-2.51	0.20

The results presented in Tables 3 and 4 are plotted in Figure 4. Following the results for the galaxies for which the ambiguity is resolved, the objects in Table 4 are plotted (with different symbols) under the assumption that a lower branch assignment is appropriate. The inclusion of these objects has no bearing on the conclusions.

There is a widespread distribution in $(O/H, \langle U \rangle)$ in Figure 4 which is a direct consequence of that in the observed (R_{23}, O_{32}) plane. While there is clearly no tight correlation between O/H and $\langle U \rangle$ as implied by observations of H II regions in HSB galaxies (e.g., Dopita & Evans 1986), an envelope of maximum $\langle U \rangle$ which decreases with increasing O/H seems to be present (cf. Campbell 1988). Such an envelope would induce an apparent $O/H - \langle U \rangle$ correlation if only the highest surface brightness H II regions are selected for observation, as these will automatically be those with the highest $\langle U \rangle$ at a given metallicity. This suggests that the correlation observed in HSB gal-

axies is a selection effect, as argued by McGaugh (1991) on theoretical grounds.

That many values of $\langle U \rangle$ exist at any given O/H is expected from simple evolutionary considerations: as an H II region ages, the stars providing the ionizing luminosity will evolve and fade, and perhaps disperse the gas through the actions of stellar winds and supernovae. Both of these will reduce $\langle U \rangle$, while O/H will not increase noticeably except at very low abundances (Kunth & Sargent 1986). Certainly, there is observational evidence that evolution is relevant (Campbell 1988; von Hippel & Bothun 1990; Caldwell et al. 1991). Hence one expects an unbiased sample to contain many $\langle U \rangle$, not just those along the envelope. This predicts (McGaugh 1992) that studies to faint levels within HSB galaxies should find that H II regions fill in the area below the envelope; i.e., they would have a distribution similar to that in Figure 4. This is confirmed in the case of M101 by the data of Scowen, Dufour, & Hester (1992). However, evolution would appear not to be the only relevant effect, as Scowen et al. (1992) find examples of low surface brightness H II regions which are also large and luminous.

The significance of the envelope is unclear. If evolution is the primary cause of the distribution in $O/H - \langle U \rangle$, then it suggests that star clusters which become the ionizing sources for extragalactic H II regions form with the same typical mass and density that will result in the $\langle U \rangle$ value along the envelope for the appropriate metallicity. This would be an important clue to the effects of metallicity on the star formation process. However, it is also possible that the clusters form over a wider variety of conditions rather than evolving to the various observed $\langle U \rangle$. If this is the case, then the envelope would represent some limiting factor on the star formation process rather than being a universal result thereof. Certainly, the envelope represents some metallicity-dependent threshold which warrants further examination.

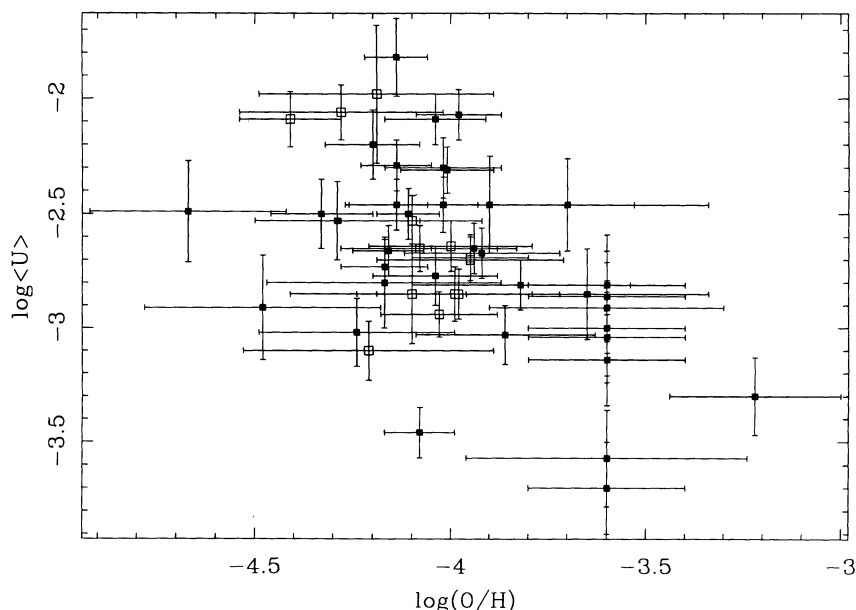


FIG. 4.—Nebular ionization parameters and oxygen abundances. This is the result of transforming Fig. 2 from (R_{23}, O_{32}) to $(O/H, \langle U \rangle)$ coordinates. As in Fig. 2, no correlation is evident, though an envelope of limiting $\langle U \rangle$ which decreases with increasing O/H does appear to be present. Solid squares are data for which the branch assignment is certain; open squares represent data for which the branch determination is ambiguous but which can reasonably be assumed to be on the lower branch (see text). The stacking of points at $\log(O/H) = -3.6$ is an artifact of the R_{23} method induced by the rapid change in the manifold of Fig. 2 near this value of the abundance.

The lack of high-metallicity, high-ionization H II regions that the envelope represents strongly suggests that the majority of objects with ambiguous abundance determinations are in fact on the lower branch. If not, these objects would lie in a region of the O/H – $\langle U \rangle$ plane not occupied by any other known extragalactic H II regions (Campbell 1988; Diaz et al. 1991), including those in LSB galaxies for which the branch assignment is certain. The only exceptions are F558-1 and UGC 6614, which have sufficiently low $\langle U \rangle$ that they do not exceed the envelope for either branch assignment, and so persist in being ambiguous (these are excluded from Fig. 4). UGC 6614 is more similar in size and morphology to the giant Malin 2 (F568-6; Bothun et al. 1990) than to the rest of the objects in the sample. If this is an indicator, then it may belong on the upper branch with Malin 2. The choice of branch makes an enormous difference in UGC 6614; it is either the most metal poor or most metal rich object in the sample. The ambiguity in this important case needs to be resolved by further observation.

4. LOCAL CONDITIONS

The H II regions provide powerful probes of the local conditions where star formation is occurring. This is of considerable interest in the more pristine systems, which may be as close to the first epoch of star formation as is observable. The mode of star formation in LSB galaxies is in some way different from that in systems which result in high surface brightnesses. In particular, the strict limits placed on molecular emission from LSB galaxies (Schombert et al. 1990) and their low H I column densities (van der Hulst et al. 1993; McGaugh et al. 1994b) imply that the formation of molecular clouds may be impaired, and thus may not be the sites of star formation as is usually presumed to be the case. An important constituent of molecular stellar cocoons is dust, which must be present in substantial quantities to shield the molecules from the interstellar radiation field, and provide sites for the formation of molecular hydrogen. The reddening toward H II regions, usually high in HSB disks (Kennicutt 1983), provides an indication of the available dust content.

A histogram of the dust content as measured by the reddening $E(B-V)$ along the line of sight to the H II regions determined from the Balmer decrements and corrected for reddening due to our own Galaxy (Burstein & Heiles 1984) is presented Figure 5. Also shown is the data of McCall et al. (1985) for Sc galaxies. Again, selection effects make the quantitative interpretation of the distribution in this histogram problematic. The two distributions do appear similar, with some tendency for LSB galaxies to contain less dust. Nevertheless, there appears to be dust in at least some LSB galaxies which could potentially be associated with molecular material.

The lack of CO detections by Schombert et al. (1990) could result either from a real lack of molecular gas, or from the breakdown of the CO/H₂ conversion at low metallicity (Maloney & Black 1988; see also Adler, Allen, & Lo 1991). The limits placed by Schombert et al. (1990) are sufficiently strict that it is unlikely that the low metallicities of LSB galaxies are the only cause of the lack of detections. Indeed, Sage et al. (1992) find no correlation between $L(\text{CO})/M(\text{H I})$ and metallicity, in which case the large H I masses of LSB galaxies should lead to easily detectable molecular gas if the latter is present in "normal" relative quantities.

While the presence of massive amounts of H₂ cannot be ruled out due to the uncertainty in the conversion factor, it

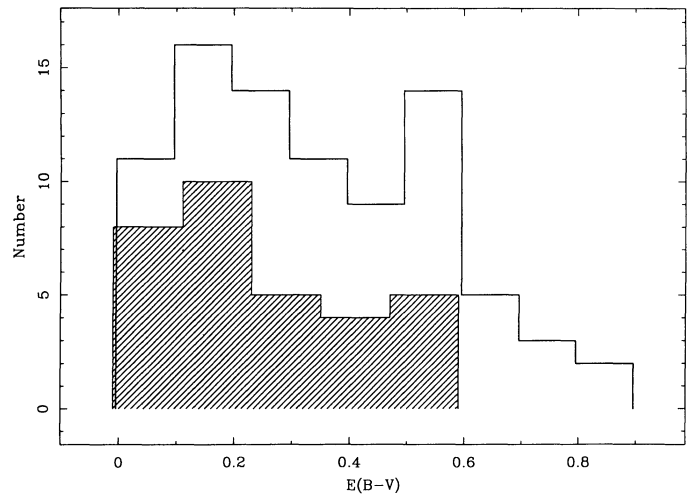


FIG. 5.—A histogram of the reddenings determined from the Balmer decrements and corrected for the galactic contribution. The hatched histogram is for LSB galaxies, while the open histogram is for HSB spirals (McCall et al. 1985).

seems likely that LSB galaxies are either devoid of molecular gas, or possess modest amounts likely to be distributed in a cloud mass spectrum different from that in HSB galaxies as a result of the low H I column densities. Any impairment of molecular cloud formation could in turn impair star formation, and lead to the current, relatively unevolved state of LSB galaxies. This supports the notion (van der Hulst et al. 1987; Kennicutt 1989; Bothun et al. 1990) that the surface density of H I is the fundamental physical quantity which controls the rate of disk evolution. Also, it should be noted that if LSB galaxies are indeed devoid of molecular gas, then the observed star formation is proceeding without the benefit of molecular clouds in sites fundamentally different from those observed in our own Galaxy.

Not only can star formation proceed without apparent molecular clouds, it also seems able to proceed before dust is produced. Figure 6 shows the reddening toward H II regions in LSB galaxies as a function of abundance. A trend of dust content increasing with metallicity is apparent (see Campbell, Terlevich, & Melnick 1986 for a similar result in BCGs). That there is a positive trend indicates that dust, like the heavy elements of which it is composed, is a stellar product which exists only in trace amounts in the least evolved systems. Indeed, that there are so many systems with low reddening immediately suggests that the low surface brightness of these galaxies is *not* induced by large internal extinction. This is corroborated by the lack of *IRAS* detections of LSB galaxies (Schombert & Bothun 1988), which further suggests that they do not contain large amounts of gray dust.

5. GLOBAL EVOLUTION

A fundamental measure of the extent of evolution that a galaxy has undergone is the degree to which it has converted the primordial gas from which it formed into stars and, through them, to metals. The latter is traditionally quantified as the metallicity Z , or mass fraction in elements heavier than hydrogen and helium. However, only within the solar system is this quantity actually measured. In studies of stars, what is usually quoted is $[\text{Fe}/\text{H}]$, the abundance of iron relative to the solar level. The conversion to Z depends on the relative abundance of all other elements to iron, usually *assumed* to be solar.

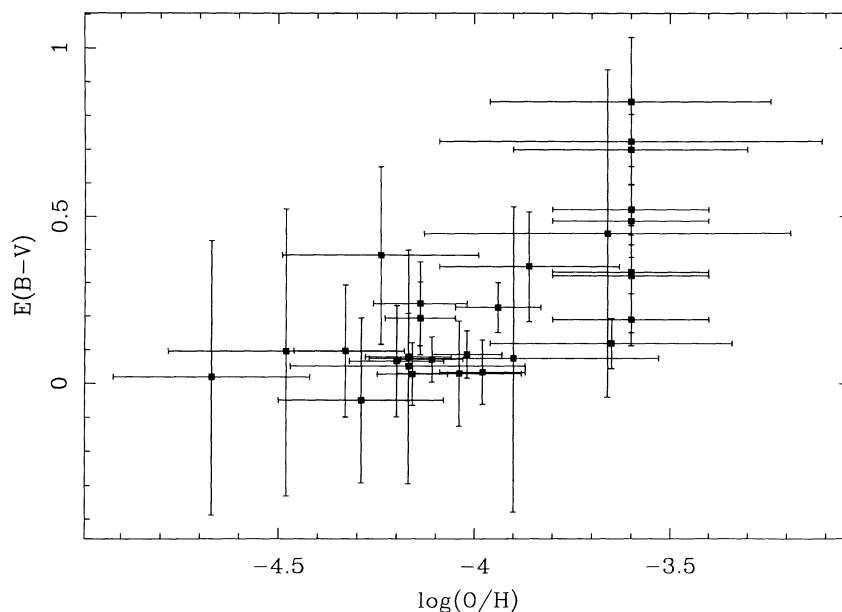


FIG. 6.—The reddening toward LSB H II regions, corrected for the galactic contribution, plotted against the oxygen abundance. Although the errors are large, there is a clear trend for the dust content to increase with metallicity.

This turns out to be a very bad assumption for low-metallicity stars in our own Galaxy, where $[\text{Fe}/\text{O}]$ is substantially subsolar (Abia & Rebolo 1989). This situation is complicated by the extreme variations that can occur in the iron to oxygen ratio depending on the star formation history of a galaxy (Gilmore & Wyse 1991). In other galaxies, the matter is further complicated in that studies of stellar metallicities are usually based on yet another element, usually magnesium (e.g., Thomsen & Baum 1987), while studies of the gas phase metallicity as probed by H II regions (such as this one) report the oxygen abundance. These differences, together with the fact that galactic absorption line strengths reflect the luminosity weighted average metallicity of a composite stellar population, while H II region abundances probe the local gas phase abundance, makes intercomparison of the results from these various methods problematic.

Of the possible approaches, the data presented here are probably best suited to the purpose at hand. The current gas phase abundance should represent the highest metallicity reached by contributions from all generations of stars. Oxygen is the most abundant of the metals, and provides the plurality of mass therein. As such, it is the best tracer of the metallicity Z . Also, it is produced in quantity exclusively by massive ($M \gtrsim 10 M_{\odot}$) stars. Thus it originates in a well-defined population and is returned to the interstellar medium on short timescales. In contrast, iron is contributed by several sources on a variety of timescales (Wheeler, Sneden, & Truran 1989).

Figure 7 shows the histogram of abundances for LSB disk galaxies. The prominent peak at $\log(\text{O}/\text{H}) = -3.6$ results in part from the uncertainty in the R_{23} method at this abundance. There really are a fair number of H II regions centered around $\log(\text{O}/\text{H}) = -3.6$, but for the larger errors at this abundance contribute to the appearance of an artificially sharp spike. This and selection effects make the quantitative interpretation of Figure 7 difficult.

Nevertheless, several points can be made. First, LSB systems cover a wide range in metallicity, over an order of magnitude in O/H . No value is obviously preferred, as it is unclear if the

distribution is truly bimodal, or merely broad with the spike inducing an artificial appearance of bimodality. A broad spectrum of slow enrichment timescales appears to be represented. This is not surprising given the diversity of size and morphology represented in this sample, and suggests that many evolutionary histories are possible which do not lead to the high surface brightness spiral galaxies which are considered "normal."

Second, the LSB galaxies with the lowest metallicities are as low as any known extragalactic objects with the exception of I Zw 18 and SBS 0335-052 (Izotov et al. 1990). Kunth &

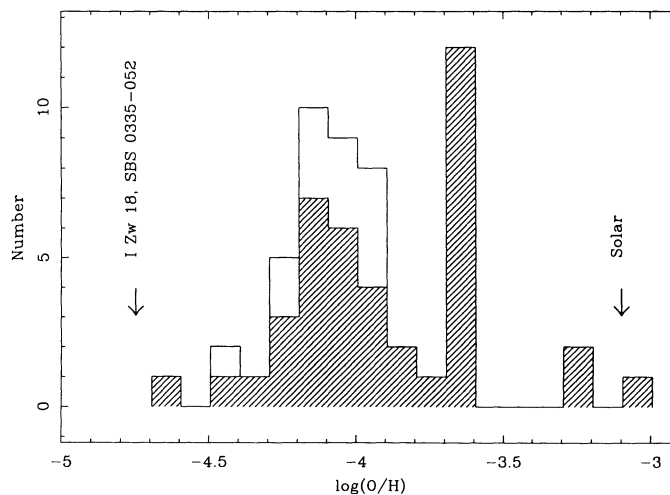


FIG. 7.—Histogram of oxygen abundances for LSB galaxies. The hatched histogram is for H II regions for which the branch assignment is certain. The open histogram represents the total sample when those H II regions with ambiguous abundance determinations which can reasonably be assumed to be on the lower branch are included. For reference, solar abundance and the abundance of the most metal poor galaxies known, I Zw 18 and SBS 0335-052, are marked with arrows. The spike at $\log(\text{O}/\text{H}) = -3.6$ is partly an artifact of the method employed to determine the oxygen abundances.

Sargent (1986) showed that an abundance of $\log(O/H) \approx -4.3$ can be reached in a very short time (a few million years) as the result of production in the first stars to explode as supernovae. They suggest that this may be the reason that extragalactic H II regions more metal poor than this are extremely rare: as soon as star formation commences, even primordial gas will be enriched to this level very rapidly. Thus it is possible that objects with $\log(O/H) \lesssim -4.3$ are undergoing their first episode of star formation. Indeed, based on abundance and color, Salzer et al. (1991) conclude that the stars producing the bulk of light of the optical component of the H I cloud in Virgo are extremely young. This object is a typical low surface brightness galaxy by the standards of this sample. Regardless of the age of the stellar population, it is clear that these galaxies are under-evolved relative to their HSB counterparts, and that selecting for low surface brightness is as effective as other means of discovering low-metallicity objects (cf. Skillman, Kennicutt, & Hodge 1989).

That these galaxies are relatively unevolved is the third, and most important, point. Virtually all LSB galaxies have substantially subsolar abundances, despite being comparable to HSB spirals in size and mass. The only galaxies containing H II regions with $\log(O/H) > -3.6$ are UGC 5709 and F568-6 (Malin 2). UGC is relatively high surface brightness ($\mu_0 = 22.49$ mag arcsec $^{-2}$), brighter than the sample median by nearly a magnitude (McGaugh 1992). Considering its extremely large size, Malin 2 may be fundamentally different from the other galaxies in this sample. Excluding these two galaxies leaves only those with $\log(O/H) < -3.6$, or $Z < 0.3 Z_{\odot}$.

6. PHYSICAL RELATIONS

Since the metallicity is a measure of the degree of evolution of a galaxy, it is of considerable interest to see if there are any

correlations between the measured abundances and other physical properties. Previous work on (predominantly HSB) disk galaxies have indicated correlations between metallicity and mass (e.g., Garnett & Shields 1987; Vila-Costas & Edmunds 1992; Oey & Kennicutt 1993), luminosity (Skillman et al. 1989 and references therein), and surface brightness (Webster & Smith 1983). Relations like these for the present sample of LSB galaxies are examined here, with relevant data taken from McGaugh (1992).

An important caveat here is that the H II region measurements provide inherently local measures of the metallicity, and there are real abundance variations across the disks of galaxies. It may therefore be inappropriate to compare locally determined abundances with global properties. To address this difficulty, varied attempts have been made to define a globally characteristic metallicity, such as the abundance at some standard radius (Garnett & Shields 1987) or a fit to the abundance gradient observed across the disk (Vila-Costas & Edmunds 1992). Unfortunately, there generally are too few H II regions in LSB galaxies to readily apply these methods. There are indications that there is little variation in some objects, and perhaps steep gradients in others. This will be investigated in greater detail in the future, together with how abundance varies with locally defined quantities (e.g., Phillipps & Edmunds 1991). For now it seems best simply to present the available data.

6.1. Size

Figure 8 shows the oxygen abundances plotted against the exponential scale lengths of the disks. These LSB galaxies cover a range of over an order of magnitude in size, most being comparable to the HSB spirals which define the Hubble sequence (McGaugh & Bothun 1994). However, they have very much lower abundances, with only the two galaxies UGC 5709 and Malin 2 discussed above having H II regions in the area log

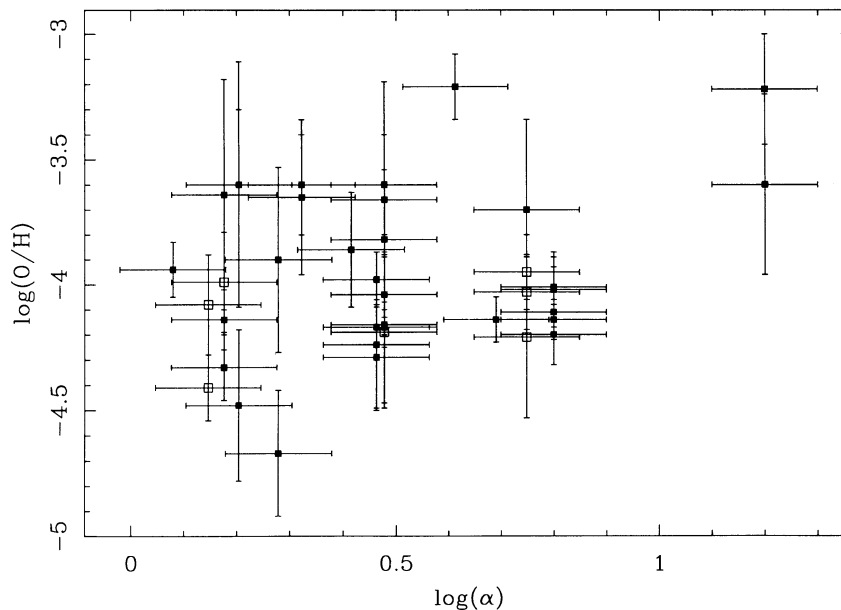


FIG. 8.—The oxygen abundances of LSB galaxies plotted against their linear size as measured by the exponential scale length α (in kpc) of their disks. The stacking of points in the vertical direction is due to the observation of multiple H II regions within a single galaxy. Although the LSB disks cover the same range in size as Freeman disks (for the assumed short distance scale), and include some quite large disks, they are much more metal poor than a “typical” solar abundance [$\log(O/H) \approx -3.1$; near the top of the graph] HSB spiral galaxy. This holds regardless of size, and there is no obvious tendency for metallicity to increase with size, especially given the incomplete sampling of H II regions in the largest galaxy (Malin 2).

(O/H) > -3.6 occupied by HSB spirals. Thus disk galaxies can be found which exist over a range of metallicities, and hence degrees of development, at *all* sizes.

6.2. Surface Brightness

Since selecting a sample for low surface brightness has resulted in the discovery of low-metallicity systems, one might expect a correlation of metallicity with surface brightness. However, there is no obvious, tight correlation between the individual H II region abundances and the *central* surface brightnesses of the disks (Fig. 9). There must be some dependence, or the selection of the sample would not have resulted in only low abundance objects. There may be some mean trend which the current data are too sparse to elucidate, or this may simply indicate the difficulty in comparing local and global quantities mentioned above. Nonetheless, it may be that the evolution of a localized portion of a stellar system is fundamentally a local phenomenon which proceeds without knowledge of the type of galaxy in which it is embedded (cf. van der Hulst et al. 1987).

6.3. Environment and Morphology

As LSB galaxies are predominantly (although not exclusively) late-type galaxies (see Schombert et al. 1992; McGaugh et al. 1994a), then to the extent that this is meaningful it may be fair to say that metallicity and morphology are correlated. However, this is only true to the same degree as it is for central surface brightness—the two go together, and result in the selection of low-metallicity objects. This does not, of course, guarantee a tight one to one correlation and may only indicate a trend with substantial scatter.

In this same general sense, surface brightness is dependent on environment (Bothun et al. 1993; Mo, McGaugh, & Bothun 1993) in the sense that LSB galaxies avoid regions of high galaxy density. Hence, more isolated galaxies are, on average, more metal poor. This result is complementary to that of

Shields, Skillman, & Kennicutt (1991), who find an enhancement of metallicity in cluster spirals. However, Henry et al. (1992) dispute this and argue that the obvious effects of cluster membership (e.g., gas stripping) do not have a serious impact on the chemical evolution of disks. Such processes are obviously unimportant in isolated LSB galaxies, so the trend of abundance with environment may point to some other underlying property, such as formation epoch (Mo et al. 1993; McGaugh et al. 1994b).

6.4. Luminosity

The relation between metallicity and luminosity is investigated in Figure 10. The oxygen abundances are plotted against the absolute magnitudes of the disk component *only*. A short ($H_0 = 100 \text{ km s}^{-1} \text{ Mpc}^{-1}$) distance scale is assumed. Lengthening the distance scale or including the contribution of any bulge component (usually minor) would have the effect of sliding the data to the right in the diagram (i.e., brighter magnitudes at fixed oxygen abundance).

There is a great deal of scatter in this diagram. Indeed, if the brightest object (Malin 2) is excluded, there is no indication of any trend of abundance with luminosity. These LSB galaxies do not follow the $M_B - Z$ relation for dwarf irregulars found by Skillman et al. (1989), nor do they form a separate sequence of their own. This cannot be ascribed to the use of locally measured abundances, as the same method was used to define the relation. Galaxies exist over a wide range of properties, and metallicity-luminosity relations should be regarded with due consideration for the sample selection effects involved (cf. Bertola, Burstein, & Buson 1993).

6.5. Mass

The situation is similar for mass (Fig. 11). No mass-metallicity relation exists for LSB disk galaxies, and there is little indication that metallicity increases at all with mass. There are objects comparable in mass to the Milky Way with

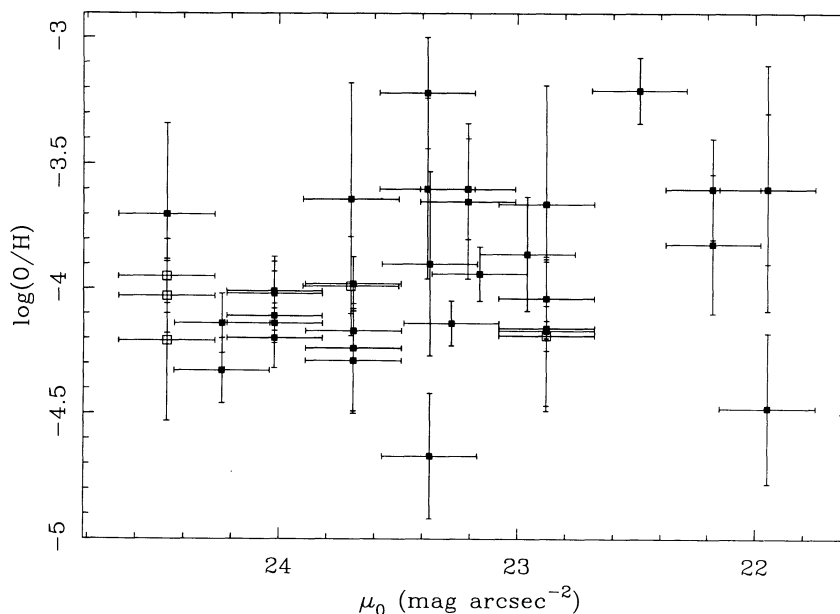


FIG. 9.—Oxygen abundance plotted against central surface brightness. Although selecting for low surface brightness has yielded low abundance objects, no direct correlation is apparent. While comparing local and global quantities is difficult (see text), this seems to indicate a complicated situation in which no single global property (such as size or surface brightness) determines the metallicity of a galaxy.

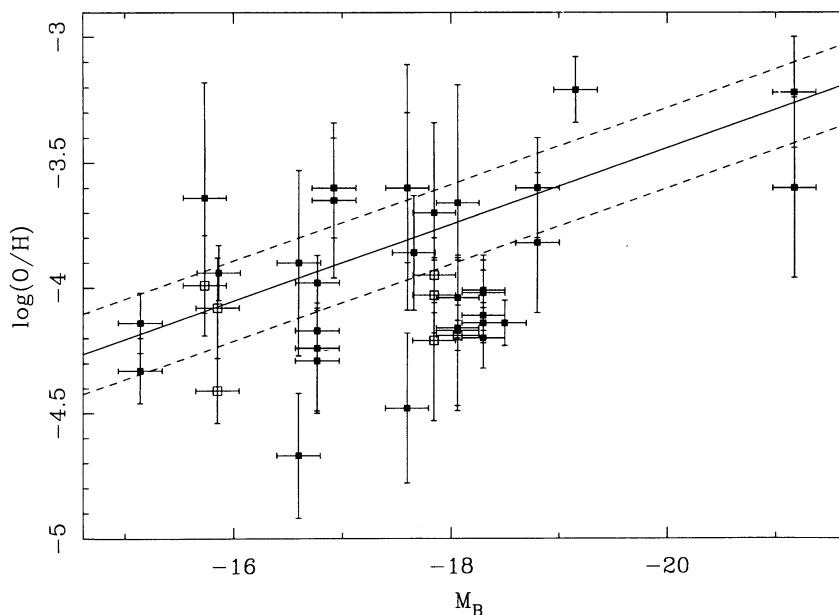


FIG. 10.—The distribution of LSB galaxies in the $O/H - M_B$ plane. Absolute magnitudes refer to the disk component only, the majority of these galaxies having little or no spheroidal component. Again, no correlation is apparent, and these LSB galaxies do not obviously follow the mean relation (*solid line*) defined by dwarf irregulars (Skillman et al. 1989). Increasing the adopted short distance scale shifts the data to the right, generally further from the 1σ range of this relation (*dashed lines*). Excluding Malin 2, which is very much brighter than the objects for which the relation is defined, the LSB data make a scatter diagram.

substantially subsolar abundances. It is not obvious that LSB galaxies would follow the trends seen by Vila-Costas & Edmunds (1992) even if a similar analysis could be performed. Certainly, the giant Malin 2 is metal poor for its mass unless it has a very steep abundance gradient *and* there is a flattening of the trend defined by HSB spirals above $10^{11} M_{\odot}$.

Considering the selection effects involved in choosing both galaxies and individual H II regions, there remains much to be done to elucidate the relationship (if any) between metallicity and the various global properties of galaxies. Low surface

brightness galaxies hold both a promise and a warning for such endeavours. Including them provides a long baseline over which the predominant effects may be distinguished. Sampling them at the low rate caused by selection effects skews our perception of the physical properties of galaxies.

7. CONCLUSIONS

Oxygen abundances in a sample of low surface brightness disk galaxies have been determined, yielding important clues to the evolutionary histories of these enigmatic objects. LSB

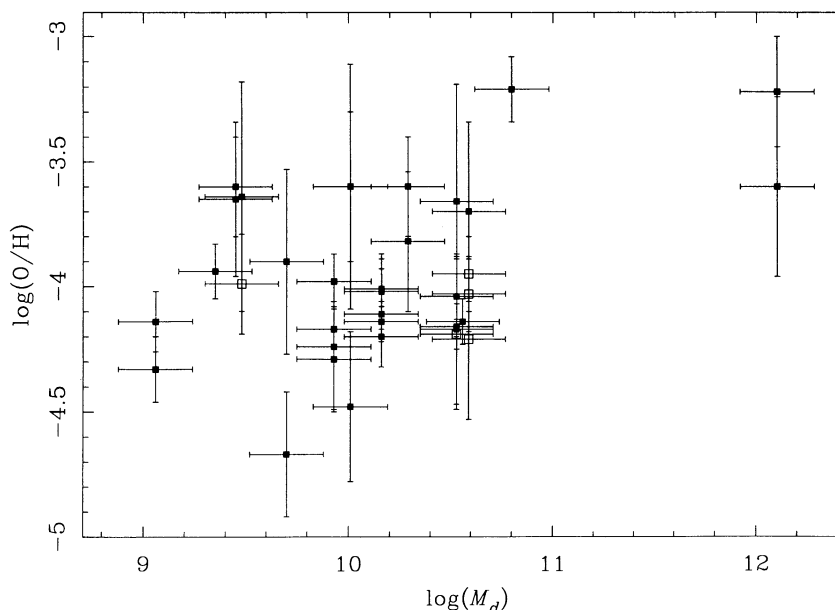


FIG. 11.—The distribution of LSB galaxies in the oxygen abundance, dynamical mass plane. Masses (in M_{\odot}) are derived from H I line widths. Grossly similar to the $O/H - M_B$ plane, no trend of metallicity increasing with mass is present, especially if the incompletely sampled giant Malin 2 is excluded.

galaxy H II regions are observed to contain massive ($M > 60 M_{\odot}$) stars, so no variation of the IMF with surface brightness is inferred, although the exact shape of the IMF is not constrained. The correlation between the nebular ionization parameter and metallicity observed in high surface brightness galaxies is not seen in this sample, but does seem to be present as an envelope of limiting maximum ionization at a given metallicity. This confirms the prediction by McGaugh (1991) that the apparent $\langle U \rangle - Z$ correlation arises from surface brightness selection effects.

LSB galaxies are low-metallicity, slowly evolving systems. The low degree of chemical enrichment confirms the inference of Bothun et al. (1990) that LSB disks evolve slowly and can remain quiescent for a Hubble time. This may result from their low H I column densities and lack of molecular gas. Indeed, the low H I column densities are likely to inhibit molecular cloud and star formation and may be the physical attribute which determines the rate of galaxy evolution.

There are trends of metallicity with surface brightness and environment in the sense that isolated, LSB objects tend to be metal poor. This holds regardless of size, with some quite large galaxies having substantially subsolar oxygen abundances. No tight correlations are apparent between metallicity and global properties like luminosity and mass. Surface brightness selection effects can mask the true range of galaxy properties, and may cause the appearance of spurious correlations between physical properties. Recovery of the entire spectrum of galaxies and galaxy properties is essential to a comprehensive understanding of galaxy formation and evolution.

I am greatly indebted to G. Bothun for his unflagging support for this project. It is a pleasure to acknowledge the insightful commentary and helpful input provided by him, R. Kennicutt, M. McCall, and J. Schombert. I am also grateful to the staffs of MDM and KPN Observatories for facilitating successful observing runs.

REFERENCES

- Abia, C., & Rebolo, R. 1989, *ApJ*, 347, 186
 Adler, D. S., Allen, R. J., & Lo, K. Y. 1991, *ApJ*, 382, 475
 Alloin, D., Collin-Souffrin, S., Joly, M., & Vigroux, L. 1979, *A&A*, 78, 200
 Bertola, F., Burstein, D., & Buson, L. M. 1993, *ApJ*, 403, 573
 Bothun, G. D., Schombert, J. M., Impey, C. D., & Schneider, S. E. 1990, *ApJ*, 360, 427
 Bothun, G. D., Schombert, J. M., Impey, C. D., Sprayberry, D., & McGaugh, S. S. 1993, *AJ*, 106, 548
 Burstein, D., & Heiles, C. 1984, *ApJS*, 54, 33
 Caldwell, N., Kennicutt, R., Phillips, A. C., & Schommer, R. A. 1991, *ApJ*, 370, 526
 Campbell, A. 1988, *ApJ*, 335, 644
 Campbell, A., Terlevich, R., & Melnick, J. 1986, *MNRAS*, 223, 811
 Diaz, A. I., Terlevich, E., Vilchez, J. M., Pagel, B. E. J., & Edmunds, M. G. 1991, *MNRAS*, 253, 245
 Dopita, M. A., & Evans, I. N. 1986, *ApJ*, 307, 431
 Edmunds, M. G., & Pagel, B. E. J. 1984, *MNRAS*, 211, 507
 Freeman, K. C. 1970, *ApJ*, 160, 811
 Garnett, D. R., & Shields, G. A. 1987, *ApJ*, 317, 82
 Gilmore, G., & Wyse, R. F. G. 1991, *ApJ*, 367, L55
 Henry, R. B. C., Pagel, B. E. J., Lasseter, D. G., & Chincarini, G. L. 1992, *MNRAS*, 258, 321
 Izotov, Yu. I., Lipovetskii, V. A., Guseva, N. G., Kniazev, A. Yu., & Stepanian, J. A. 1990, *Nature*, 343, 238
 Kennicutt, R. C. 1983, *ApJ*, 272, 54
 ———. 1989, *ApJ*, 344, 685
 Kunth, D., & Sargent, W. L. W. 1986, *ApJ*, 300, 496
 Luppino, G. A. 1989, *PASP*, 101, 931
 Maloney, P., & Black, J. H. 1988, *ApJ*, 325, 389
 Matteucci, F. 1986, *PASP*, 98, 973
 McCall, L. M., Rybski, P. M., & Shields, G. A. 1985, *ApJS*, 57, 1
 McGaugh, S. S. 1991, *ApJ*, 380, 140
 ———. 1992, Ph.D. thesis, University of Michigan
 McGaugh, S. S., & Bothun, G. D. 1994, *AJ*, in press
 McGaugh, S. S., Bothun, G. D., & Schombert, J. M. 1994a, *AJ*, submitted
 McGaugh, S. S., Bothun, G. D., van der Hulst, J. M., & Schombert, J. M. 1994b, in preparation
 Mo, H. J., McGaugh, S. S., & Bothun, G. D. 1994, *MNRAS*, in press
 Nilson, P. 1973, Uppsala General Catalog of Galaxies (Uppsala, Sweden: Societatis Scientiarum Upsaliensis) (UGC)
 Oey, M. S., & Kennicutt, R. C. 1993, *ApJ*, 411, 137
 Olofsson, K. 1989, *A&AS*, 80, 317
 Osterbrock, D. E. 1989, *Astrophysics of Gaseous Nebulae and Active Galactic Nuclei* (Mill Valley, CA: University Science Books)
 Pagel, B. E. J., & Edmunds, M. G. 1981, *ARA&A*, 19, 77
 Pagel, B. E. J., Edmunds, M. G., Blackwell, D. E., Chun, M. S., & Smith, G. 1979, *MNRAS*, 193, 219
 Peimbert, M., Sarmiento, A., & Fierro, J. 1991, *PASP*, 103, 815
 Phillipps, S., & Edmunds, M. G. 1991, *MNRAS*, 251, 84
 Romanishin, W., Strom, K. M., & Strom, S. E. 1983, *ApJS*, 53, 105
 Sage, L. J., Salzer, J. J., Loose, H.-H., & Henkel, C. 1992, *A&A*, 265, 19
 Salzer, J. J., Alighieri, S. D. S., Matteucci, F., Giovanelli, R., & Haynes, M. P. 1991, *AJ*, 101, 1258
 Savage, B. D., & Mathis, J. S. 1979, *ARA&A*, 17, 73
 Schombert, J. M., & Bothun, G. D. 1988, *AJ*, 95, 1389
 Schombert, J. M., Bothun, G. D., Impey, C. D., & Mundy, L. G. 1990, *AJ*, 100, 1523
 Schombert, J. M., Bothun, G. D., Schneider, S. E., & McGaugh, S. S. 1992, *AJ*, 103, 1107
 Scowen, P. A., Dufour, R. J., & Hester, J. J. 1992, *AJ*, 104, 92
 Shields, G. A., Skillman, E. D., & Kennicutt, R. C. 1991, *ApJ*, 371, 82
 Silva, D. R. 1991, Ph.D. thesis, University of Michigan
 Skillman, E. D. 1989, *ApJ*, 347, 883
 Skillman, E. D., Kennicutt, R. C., & Hodge, P. W. 1989, *ApJ*, 347, 875
 Terlevich, R. 1985, in *Star Forming Dwarf Galaxies*, ed. D. Kunth, T. X. Thuan, & J. J. T. Van (Paris: Editions Frontières), 395
 Thomsen, B., & Baum, W. A. 1987, *ApJ*, 315, 460
 Torres-Peimbert, S., Peimbert, M., & Fierro, J. 1989, *ApJ*, 345, 186
 Tyson, N. D., & Scalzo, J. M. 1988, *ApJ*, 329, 618
 van der Hulst, J. M., Skillman, E. D., Kennicutt, R. C., & Bothun, G. D. 1987, *A&A*, 177, 63
 van der Hulst, J. M., Skillman, E. D., Smith, T. R., Bothun, G. D., McGaugh, S. S., & de Blok, W. J. G. 1993, *AJ*, 106, 548
 Vila-Costas, M. B., & Edmunds, M. G. 1992, *MNRAS*, 259, 121
 ———. 1993, *MNRAS*, in press
 von Hippel, T., & Bothun, G. 1990, *AJ*, 100, 403
 Webster, B. L., Longmore, A. J., Hawarden, T. G., & Mebold, U. 1983, *MNRAS*, 205, 643
 Webster, B. L., & Smith, M. G. 1983, *MNRAS*, 204, 743
 Wheeler, J. C., Sneden, C., & Truran, J. W. 1989, *ARA&A*, 27, 279